eLIFE elifesciences.org

RESEARCH ARTICLE

Figures and figure supplements

BAD and K_{ATP} channels regulate neuron excitability and epileptiform activity

Juan Ramón Martínez-François *et al*

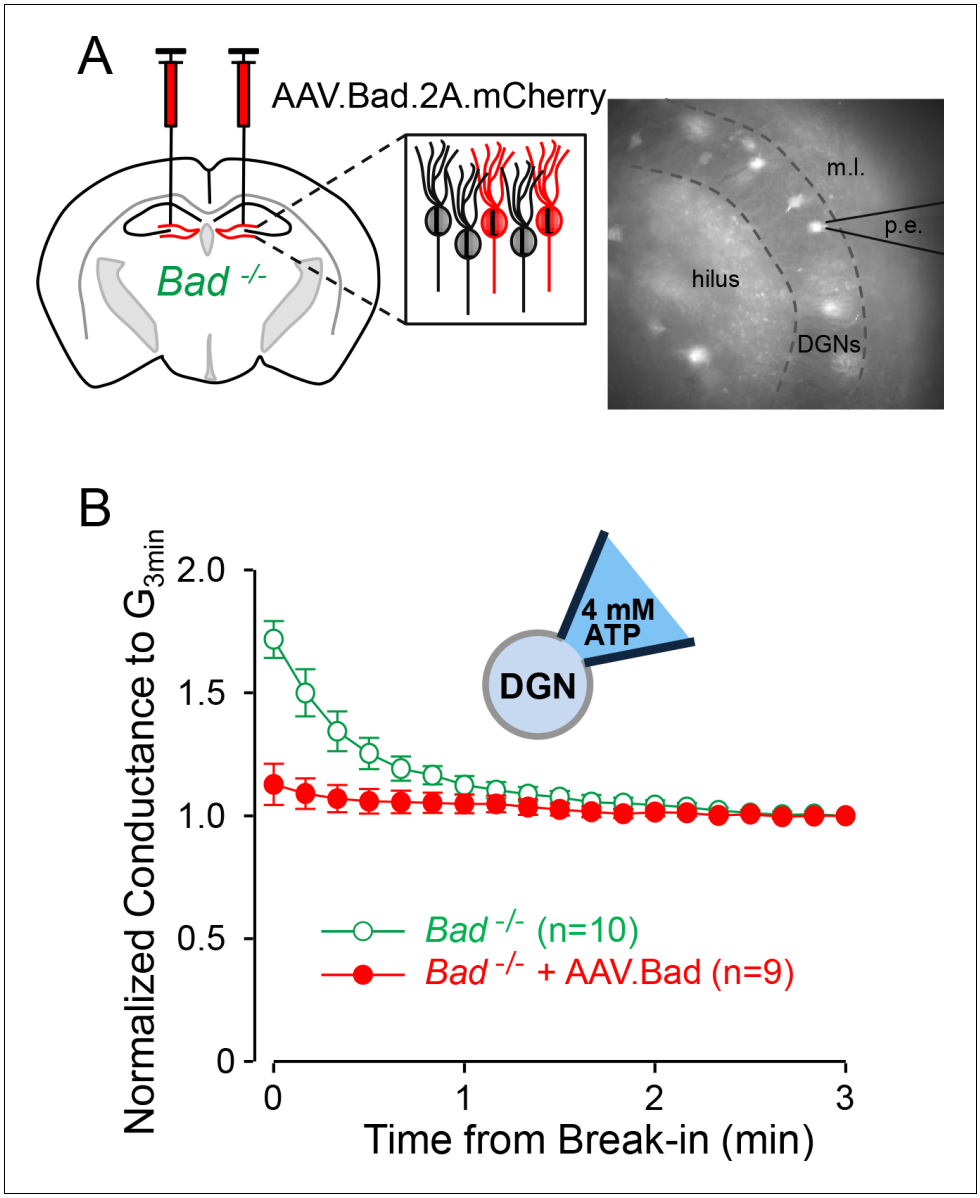

Figure 1. Effect of BAD on K_{ATP} channels is cell-autonomous. (**A**) Left: schematic representation of intracranial injection of AAV.Bad.2A.mCherry in the hippocampus of *Bad*$^{-/-}$ mice to reconstitute BAD expression in mCherry labeled cells. Right: epifluorescence picture of a BAD-reconstituted *Bad*$^{-/-}$ DGN being recorded with a patch electrode (p.e.) in the whole-cell mode. Regions observed in picture: hilus, dentate granule cell layer (DGNs) and molecular layer (m.l.). (**B**) 'Washdown' of an initially high K_{ATP} conductance, with high ATP (4 mM) in the patch electrode, seen in *Bad*$^{-/-}$ but not BAD-reconstituted *Bad*$^{-/-}$ cells. The time course of slope conductance measured during whole-cell recording was normalized to the value 3 min after break-in. Data are presented as mean ± SEM.

DOI: https://doi.org/10.7554/eLife.32721.002

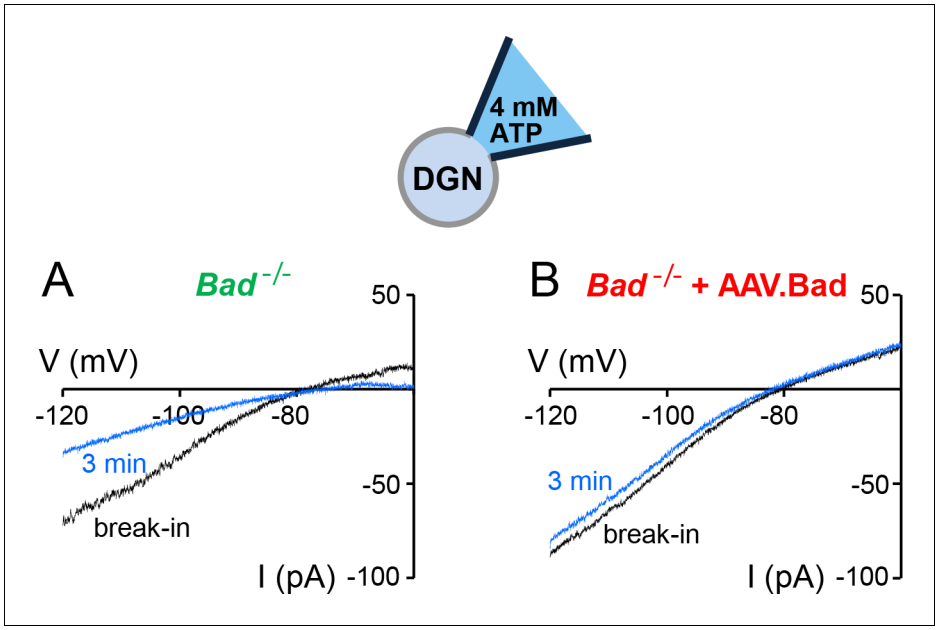

Figure 1—figure supplement 1. 'Washdown' of K_{ATP} channel conductance in *Bad*$^{-/-}$ or BAD-reconstituted DGNs. Representative whole-cell current traces with high ATP (4 mM) in the patch electrode in a *Bad*$^{-/-}$ (**A**) or a BAD-reconstituted DGN (**B**). As the high ATP concentration washed into the cell, the conductance decreased in the *Bad*$^{-/-}$ cell (A, compare initial black trace to blue trace after 3 min of recording) but remained of comparable magnitude when BAD was reconstituted via AAV.

DOI: https://doi.org/10.7554/eLife.32721.003

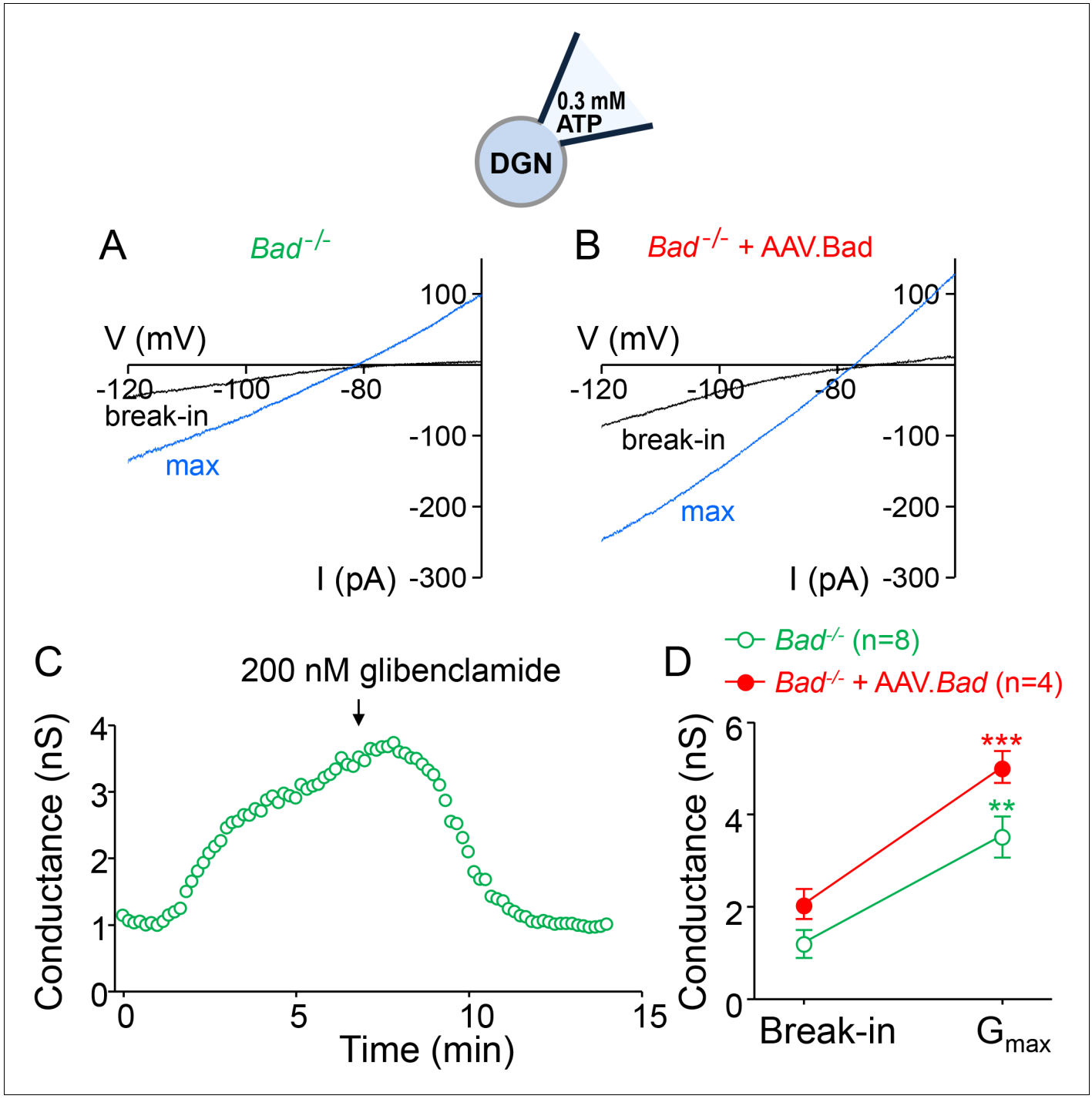

Figure 1—figure supplement 2. Total activatable whole-cell K_{ATP} conductance is mostly unaffected by overexpressing BAD in $Bad^{-/-}$ DGNs. (**A**,**B**) Representative whole-cell current traces with low ATP (0.3 mM) in the patch electrode (p. (**e**).) in a $Bad^{-/-}$ (**A**) or a BAD-reconstituted (**B**) DGN at the moment of break-in (black traces) or after current had maximally increased (blue traces) due to disinhibition of K_{ATP} channels. (**C**) Typical whole-cell K_{ATP} conductance time course with low ATP in the patch electrode in a $Bad^{-/-}$ DGN. Slope conductance gradually increased upon breaking into the cell as K_{ATP} channels became uninhibited. This K_{ATP} conductance 'run-up' was reversed by application of 200 nM glibenclamide (arrow), a K_{ATP} channel inhibitor. (**D**) Maximum activatable K_{ATP} conductance (mean ±SEM) determined from the difference between the slope conductance at the time of break-in and after conductance run-up (G_{max}), with low ATP (0.3 mM) in the patch electrode, for $Bad^{-/-}$ and BAD-reconstituted $Bad^{-/-}$ as indicated. **p<0.01; ***p<0.001; two-tailed Student's *t*-test.

DOI: https://doi.org/10.7554/eLife.32721.004

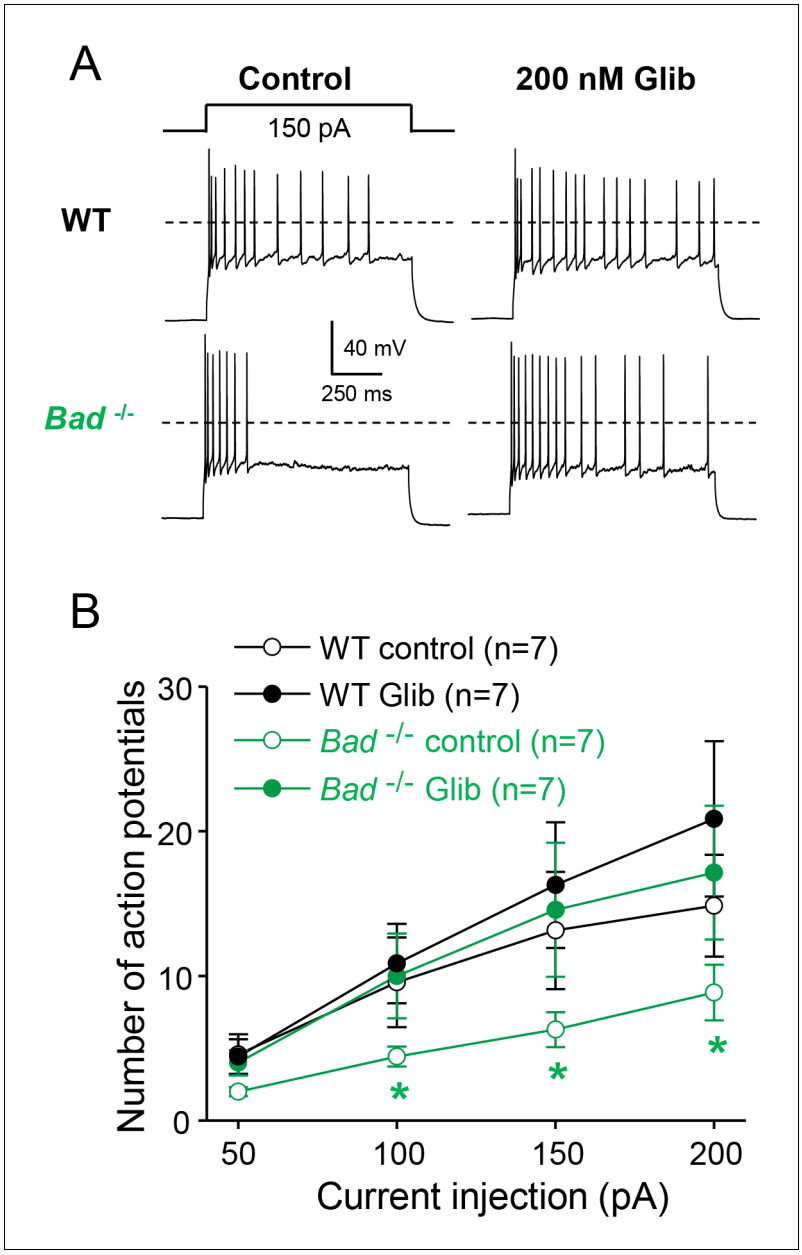

Figure 2. Dentate granule neurons lacking BAD are less excitable. (**A**) *Bad*$^{-/-}$ DGNs fire fewer action potentials that wild-type (WT), and 200 nM glibenclamide reverses *Bad* knockout effect on DGN excitability. Representative perforated-patch voltage recordings in response to a 1 s, 150 pA current pulse for WT and *Bad*$^{-/-}$ DGNs, in the presence or absence of 200 nM glibenclamide, as indicated. Dotted lines indicate 0 mV. (**B**) Glibenclamide application increases firing of *Bad*$^{-/-}$ DGNs but not that of WT. Number of action potentials (mean ± SEM) plotted against magnitude of current injection pulse. *p<0.05; 1-way ANOVA.

DOI: https://doi.org/10.7554/eLife.32721.005

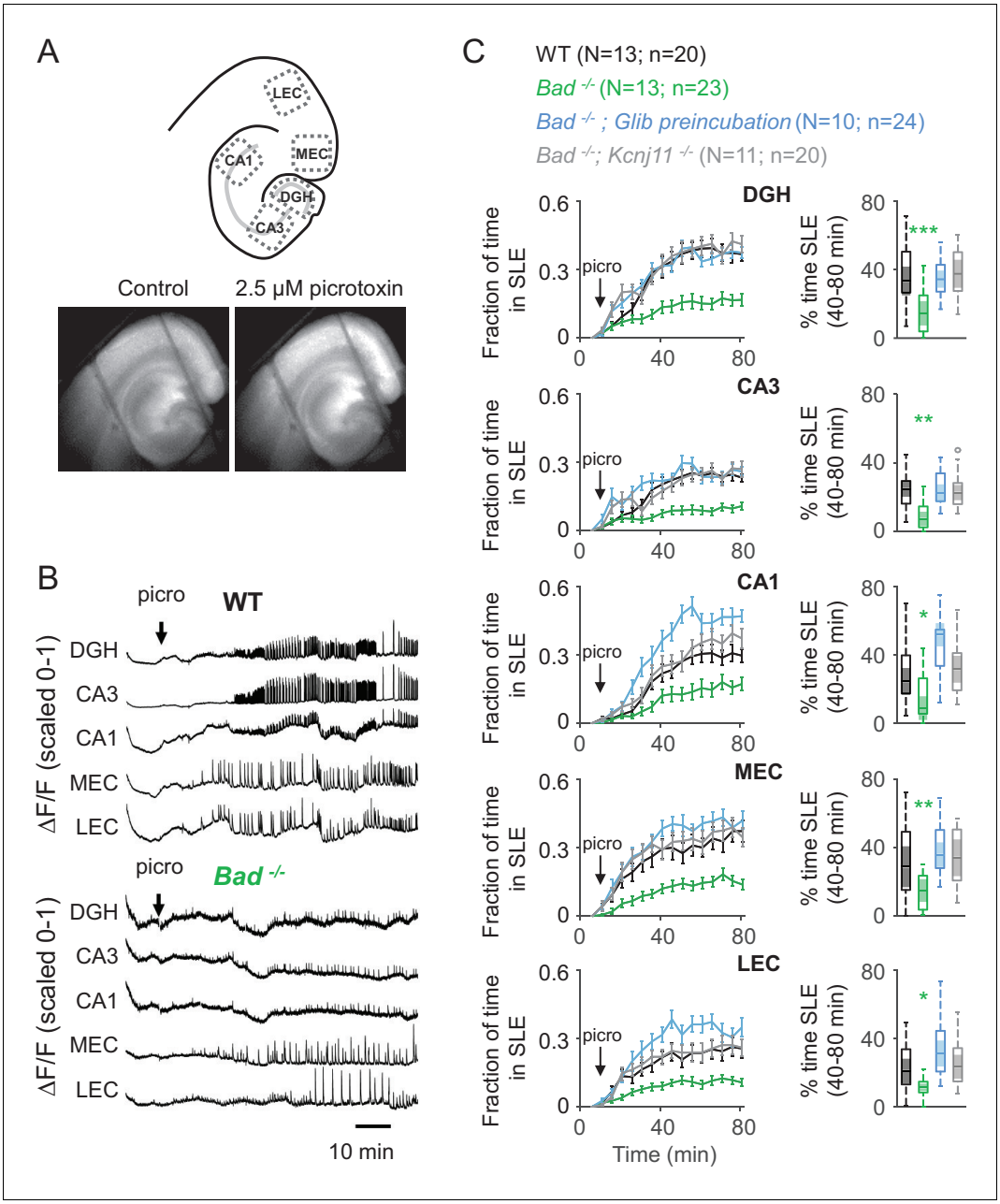

Figure 3. Deletion of BAD reduces picrotoxin-elicited epileptiform activity. (**A**) Top: Schematic representation of the analyzed regions of interest in EC-HC acute slices; dentate gyrus/hilus (DGH), CA3, CA1, medial entorhinal cortex (MEC) and lateral entorhinal cortex (LEC). Bottom: representative epifluorescence images of an EC-HC slice expressing GCaMP6f in ACSF (Control; left) or in the presence of 2.5 µM picrotoxin as a SLE is occurring (right). (**B**) Picrotoxin application triggers SLEs. Representative ΔF/F traces (normalized from 0 to 1) in wild-type (WT; top) or *Bad*$^{-/-}$ (bottom) slices for the indicated regions of interest. The arrows indicate extracellular application of 2.5 µM picrotoxin in the extracellular bath. (**C**) Genetic deletion of BAD reduced the time EC-HC slices spent in SLEs, and this effect was mediated by K_{ATP} channels. Fraction of time spent in SLEs (mean ± SEM) plotted versus time (left column) or percent time in SLEs calculated from the 40–80 min range when seizure-like activity plateaus (right column) for each region of interest analyzed, and genotypes and conditions specified. *p<0.05; **p<0.005; ***p<0.0005; 1-way ANOVA.

DOI: https://doi.org/10.7554/eLife.32721.006

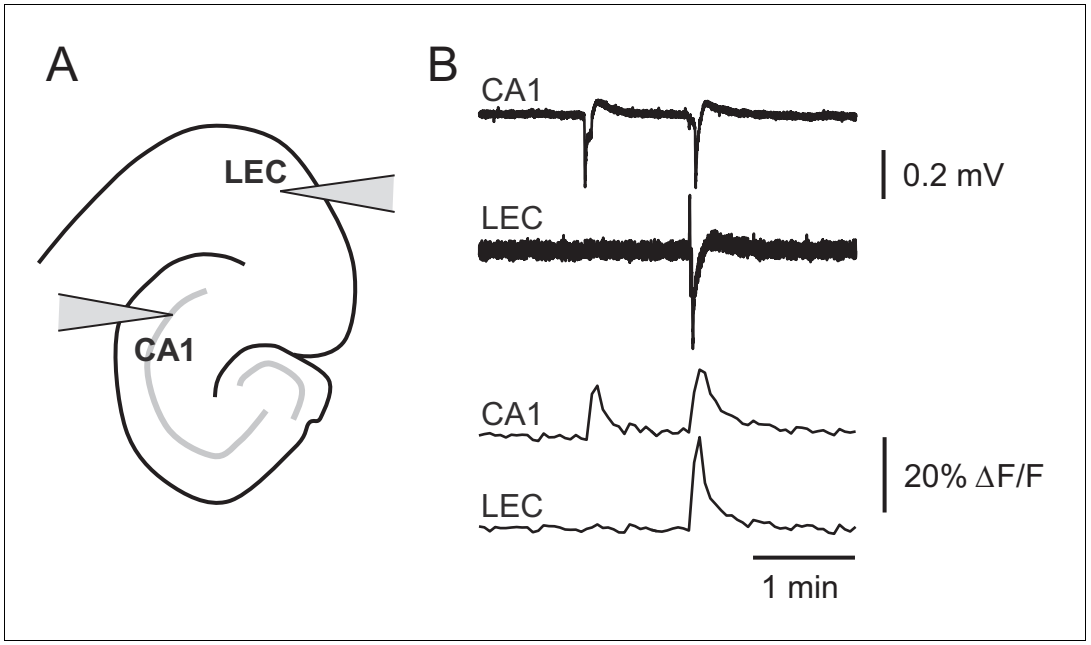

Figure 3—figure supplement 1. Picrotoxin-triggered changes in GCaMP6f fluorescence intensity correspond to stereotypical epileptiform field potentials. (**A**) Schematic representation of extracellular field potential electrode placement in CA1 or lateral entorhinal cortex (LEC). (**B**) Changes in GCaMP6f fluorescence faithfully represent picrotoxin-triggered field potentials. Representative field potential traces (upper) or $\Delta F/F$ traces (lower) simultaneously recorded in CA1 or LEC in the presence of 2.5 μM picrotoxin.

DOI: https://doi.org/10.7554/eLife.32721.007

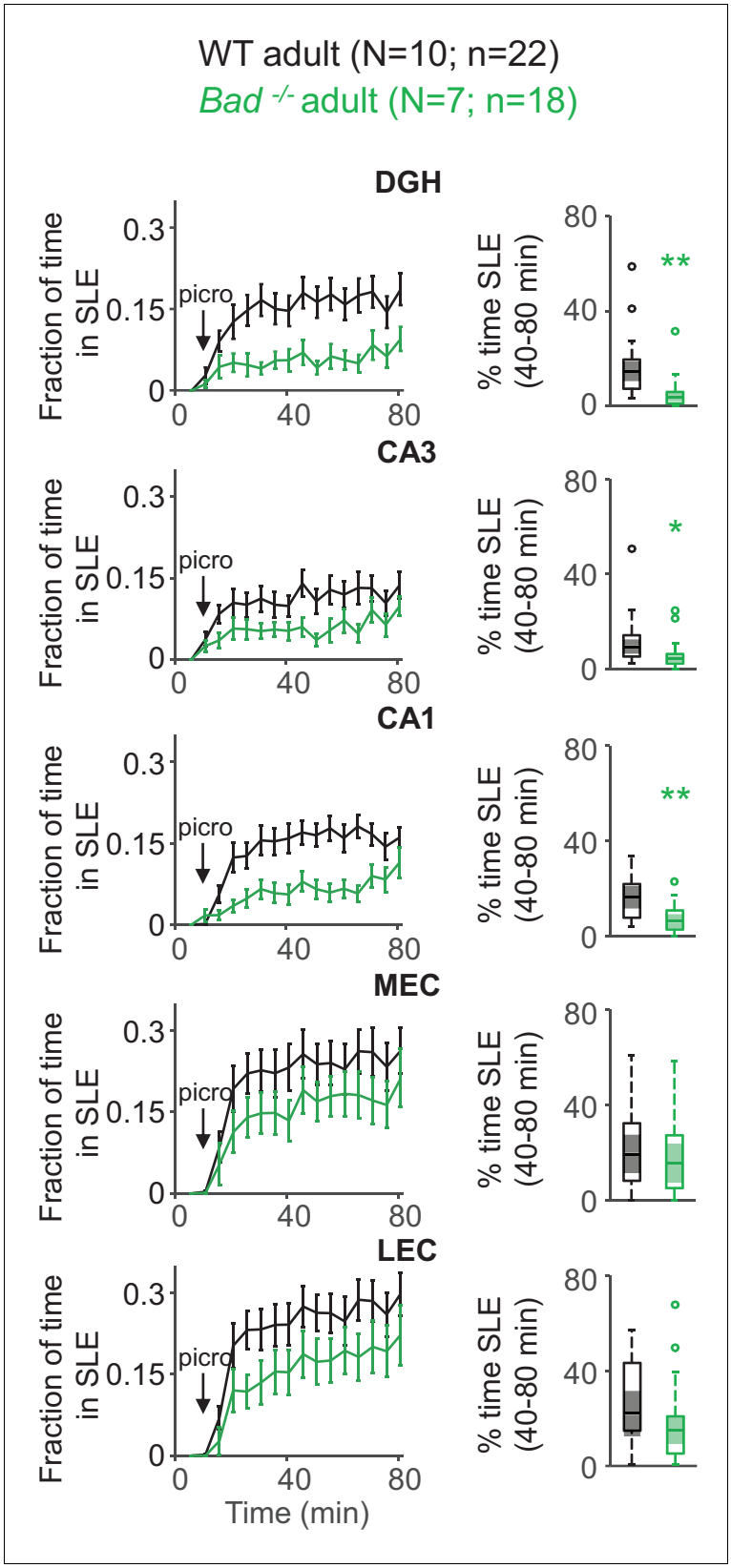

Figure 4. Deletion of BAD decreases picrotoxin-triggered seizure-like activity in adult EC-HC slices. Genetic deletion of BAD reduced the time hippocampal regions spent in SLEs in adult slices. Left column: fraction of time spent in SLEs (mean ± SEM) plotted versus time. The arrows indicate extracellular application of 50 µM picrotoxin

Figure 4 continued on next page

Figure 4 continued

in the extracellular bath. Right column: percent time in SLEs calculated from the 40–80 min range when seizure-like activity plateaus for each region of interest analyzed and genotypes specified. *p<0.05; **p<0.005; two-tailed Student's *t*-test.

DOI: https://doi.org/10.7554/eLife.32721.009

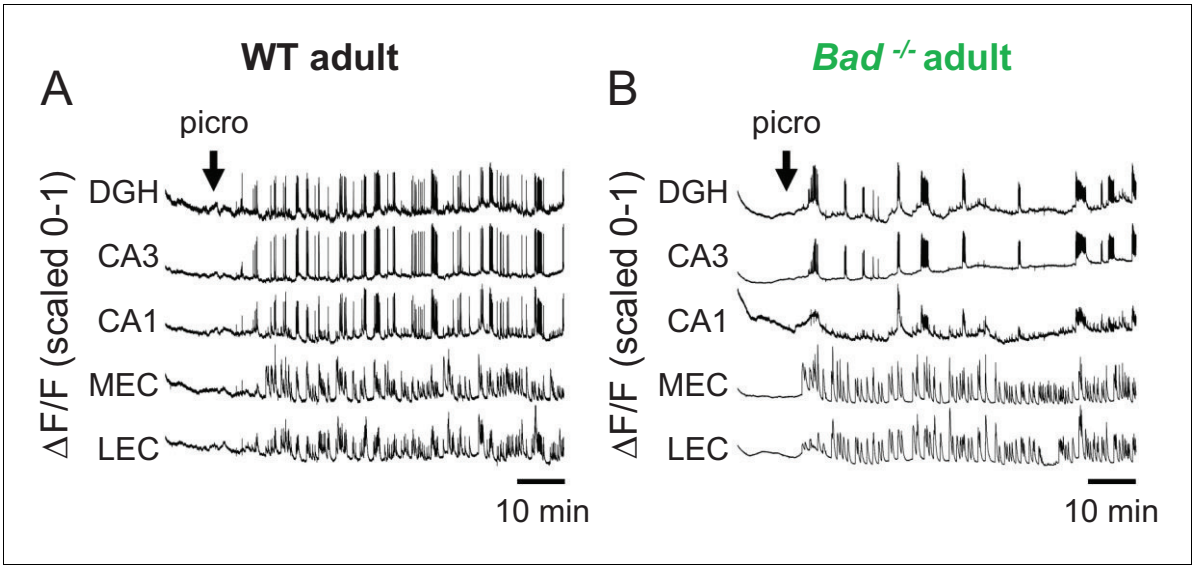

Figure 4—figure supplement 1. Picrotoxin-elicited epileptiform activity in adult EC-HP slices. Picrotoxin application triggers SLEs in adult EC-HP slices. Representative ΔF/F traces (normalized from 0 to 1) in adult wild-type (**A**) or adult *Bad*$^{-/-}$ (**B**) slices for the indicated regions of interest. The arrows indicate extracellular application of 50 μM picrotoxin in the extracellular bath.

DOI: https://doi.org/10.7554/eLife.32721.010

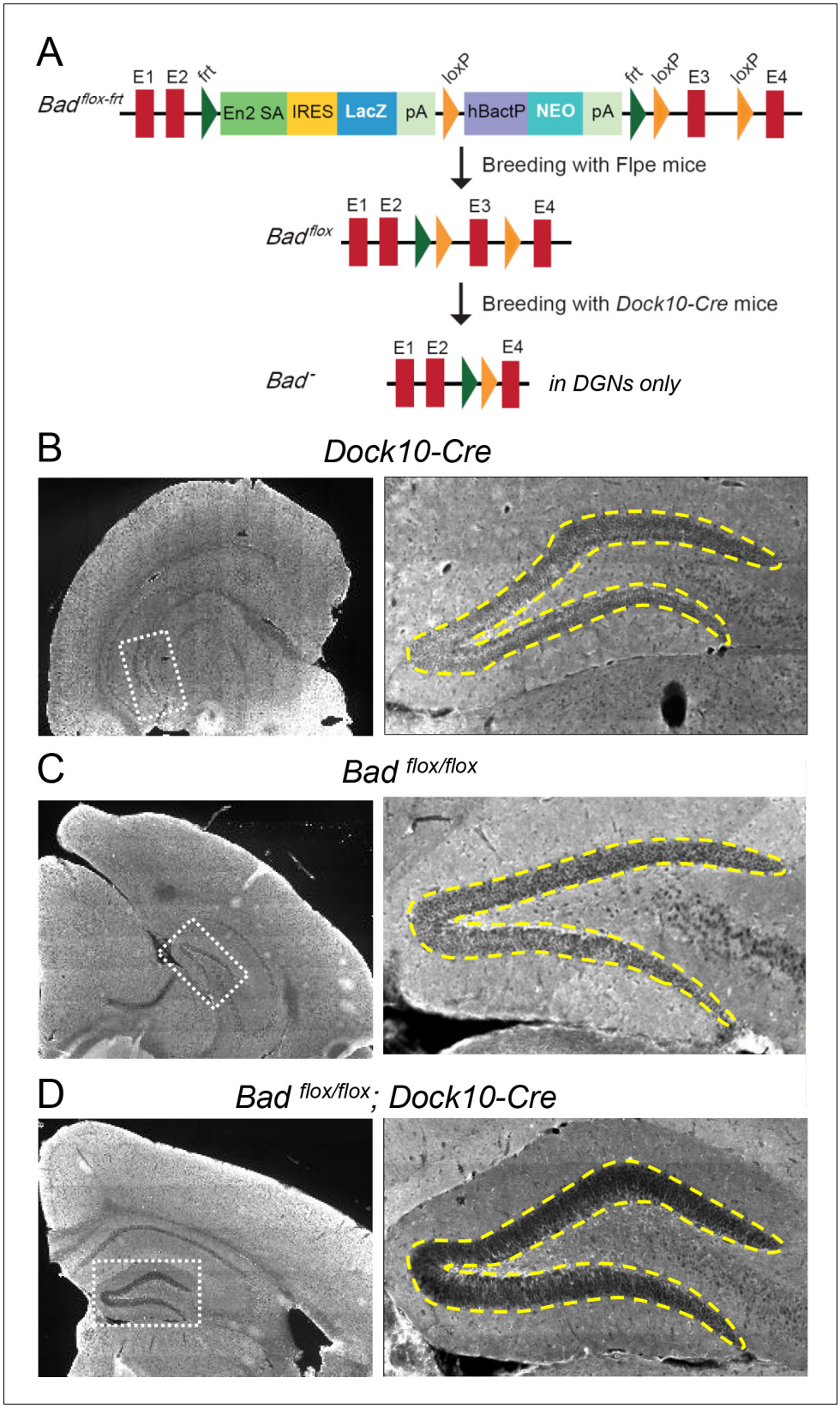

Figure 5. Targeted knockout of *Bad* expression in the dentate gyrus but not in the rest of the hippocampus. (**A**) Schematic illustration of the targeting construct and strategy to generate the conditional Bad^{flox} allele. *Abbreviations*: En2 SA: En2 splice acceptor; IRES: Internal ribosomal entry site; pA: polyadenylation sequence; Frt:

Figure 5 continued on next page

Figure 5 continued

Flipase (Flpe) recombinase target; loxP: Cre recombinase target; hBactP: human beta actin promoter; NEO: neomycin resistance gene. (**B, C, D**) Immunostaining for BAD in brain coronal sections from mice of the specified genotypes. Notice lack of BAD expression only in DGNs from *Bad*$^{flox/flox}$*; Dock10-Cre* brain. In the right column dashed line area demarcates the DGN cell body layer. Also notice the lower fluorescence intensity in the entire molecular layer of the dentate gyrus (containing the dendrites of the DGNs) in *Bad*$^{flox/flox}$*; Dock10-Cre* compared to the parental genotypes.

DOI: https://doi.org/10.7554/eLife.32721.011

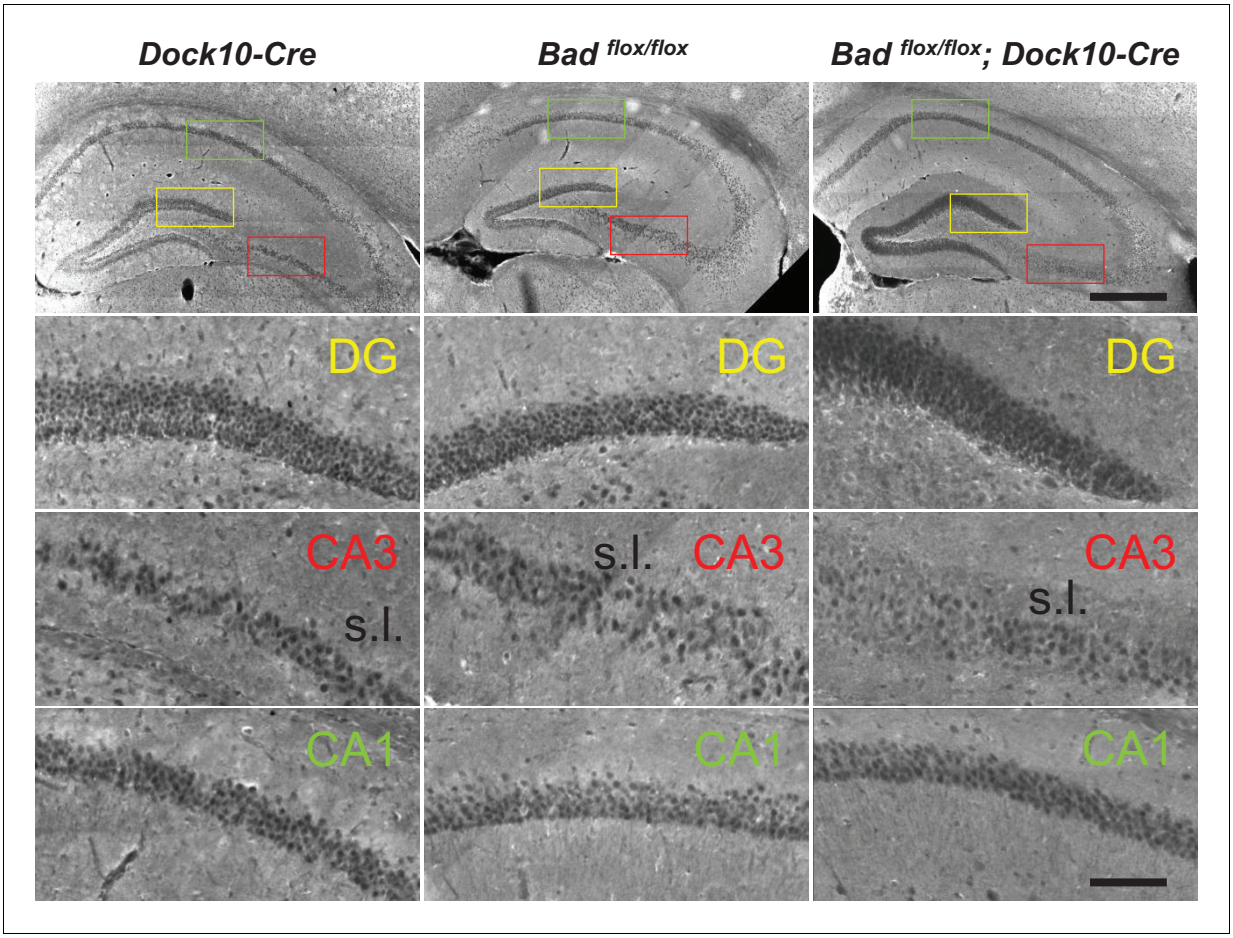

Figure 5—figure supplement 1. Targeted knockout of *Bad* expression in the dentate gyrus: coronal sections. Immunostaining for BAD in brain coronal sections from mice of the specified genotypes. BAD expression is only absent in DGNs from *Bad*$^{flox/flox}$*; Dock10-Cre* brain. Notice decreased BAD staining in stratum lucidum (s.l.) of *Bad*$^{flox/flox}$*; Dock10-Cre* CA3; this region contains the mossy fiber axons of the DGNs. Color squares in the top row indicate the expanded areas in the other rows as indicated. Scale bars: 500 μm (top) and 100 μm (bottom).

DOI: https://doi.org/10.7554/eLife.32721.012

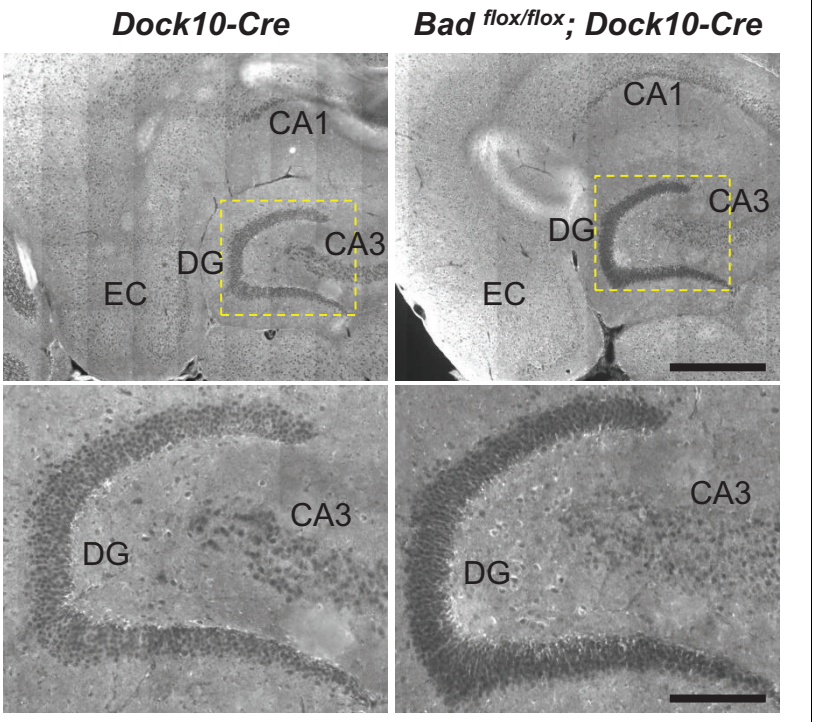

Figure 5—figure supplement 2. Targeted knockout of *Bad* expression in the dentate gyrus: horizontal sections. Immunostaining for BAD in brain horizontal sections from mice of the specified genotypes. BAD expression is only absent in DGNs from *Bad*$^{flox/flox}$; *Dock10-Cre* brain. Notice appreciable BAD expression in EC of both genotypes. Dashed yellow squares in top row indicate the expanded areas in bottom row. Scale bars: 500 μm (top) and 175 μm (bottom).

DOI: https://doi.org/10.7554/eLife.32721.013

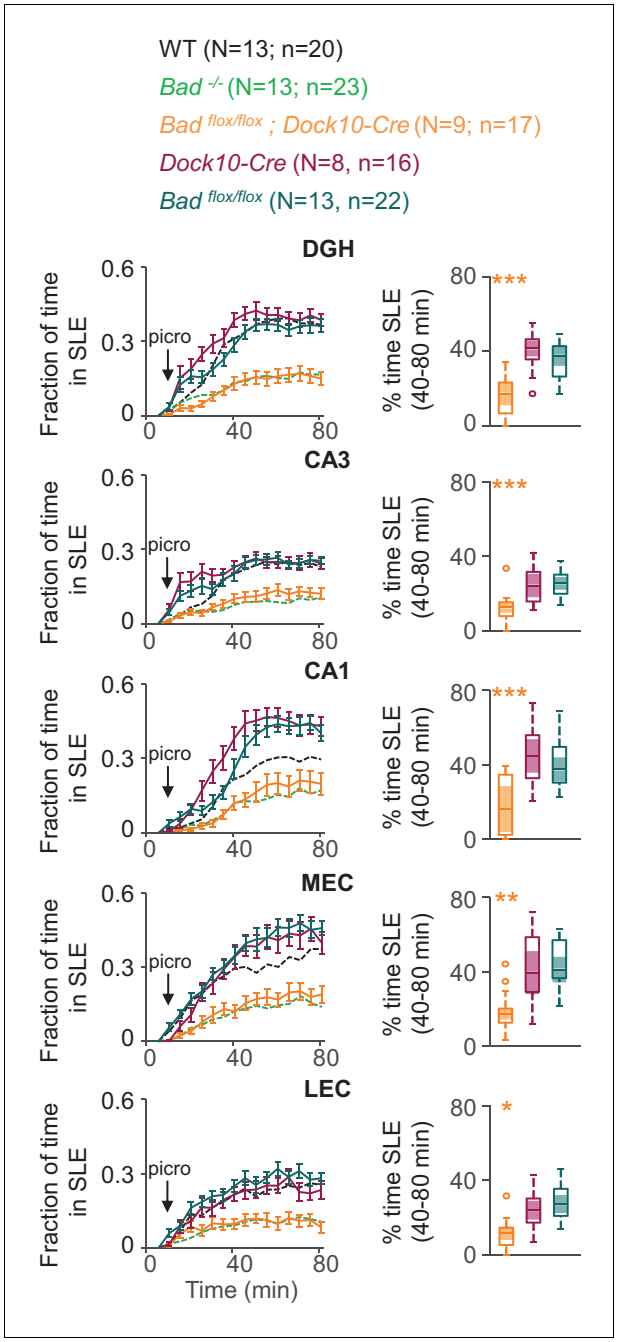

Figure 6. DGN-specific BAD ablation is sufficient to reduce seizure-like activity. Genetic deletion of *Bad* in DGNs alone (*Bad*$^{flox/flox}$; *Dock10-Cre*, orange) reduced the time hippocampal regions spent in SLEs in adult slices. Left column: fraction of time spent in SLEs (mean ± SEM) for *Bad*$^{flox/flox}$; *Dock10-Cre* (orange), *Dock10-Cre* (dark magenta) or *Bad*$^{flox/flox}$ (teal) plotted versus time. For comparison, WT (black) and *Bad*$^{-/-}$ (green) data are reproduced from ***Figure 3*** as dashed lines without error bars. Right column: percent time in SLEs calculated from the 40–80 min range when seizure-like activity plateaus for each region of interest analyzed. *p<0.05; **p<0.005; ***p<0.0005; 1-way ANOVA.

DOI: https://doi.org/10.7554/eLife.32721.014